Journal of the Physical Society of Japan
Vol. 74, No. 1, January, 2005, pp. 88–94

The Kondo Effect Enhanced by State Degeneracy

Satoshi SASAKI* and Seigo TARUCHA[1]

NTT Basic Research Laboratories, NTT Corporation, 3-1 Morinosato-Wakamiya, Atsugi, Kanagawa 243-0198
[1]ERATO, Mesoscopic Correlation Project and Department of Applied Physics, University of Tokyo, 7-3-1, Hongo, Bunkyo-ku, Tokyo 113-0033

(Received September 17, 2004)

The Kondo effect associated with state degeneracy is studied for a two-dimensional harmonic quantum dot. State degeneracies between a spin singlet and triplet states, between two spin doublet states, and between a spin doublet and quadruplet states are induced by magnetic field. For the first two degenracies, strong enhancement of the Kondo effect is observed. The estimated Kondo temperature for the "doublet–doublet" degeneracy with an odd electron number is similar to that for the "singlet–triplet" degeneracy with an even electron number, indicating that a total of four-fold spin and orbital degeneracy for both cases accounts for the similar enhancement of the Kondo temperature. The Kondo effect generally gives rise to enhanced conductnace and a zero-bias *peak* of differential conductance in the Coulomb valley. In contrast, enhacned conductance but a zero-bias *dip* is observed for the third "doublet–quadruplet" degeneracy. This can be due to Zeeman splitting but no clear interpretation is reached yet.

KEYWORDS: quantum dot, Kondo effect, spin configuration, transport properties, many-body effect, singlet–triplet degeneracy, doublet–doublet degeneracy
DOI: 10.1143/JPSJ.74.88

1. Introduction

Since the concept of the Kondo effect was established in 1964 by Professor Kondo,[1)] a number of experimental and theoretical studies have been performed on various kinds of bulk metals to explore the many-body effects in the condensed matter physics. The interest in the Kondo effect was renewed when the Kondo effect was observed in 1998 for semiconductor quantum dot devices.[2)] These devices have enabled studies on the Kondo effect associated with a single isolated magnetic impurity or a spin-half electron trapped in a quantum dot, instead of a large ensemble of magnetic impurities in bulk metal. In addition, various parameters that influence the many-body effects are handled in a controlled manner in quantum dot devices. These advantages of quantum dots have opened up new approaches to the Kondo physics, resulting in a number of novel findings.

The Kondo effect in quantum dots arises from the singlet coupling between a localized electron spin in a dot and Fermi seas of the tunnel-coupled contact leads.[3)] Figure 1(a) shows an energy diagram of such a quantum dot having one spin-up electron at the uppermost level whose energy is ε_0. The total spin $S = 1/2$ for this dot. The coupling of the electron spin to Fermi seas in the contact leads has tunnel rates, Γ_L and Γ_R, for the left and right barriers, respectively. ε_0 is adjusted so that $\varepsilon_0 < E_F < \varepsilon_0 + U$, where E_F is the Fermi energy and U is the charging energy. Then, the first-order tunneling through the dot is inhibited because of U (Coulomb blockade). However, when the temperature is lowered to $\sim T_K$ (Kondo temperature), the electron in the dot forms a singlet coupling with a spin-down electron in the lead, and concurrent tunneling of these two electrons contributes to a net electron transfer between the source and drain leads as depicted in Fig. 1(a). At the same time, a Kondo resonance peak appears in the local density of states

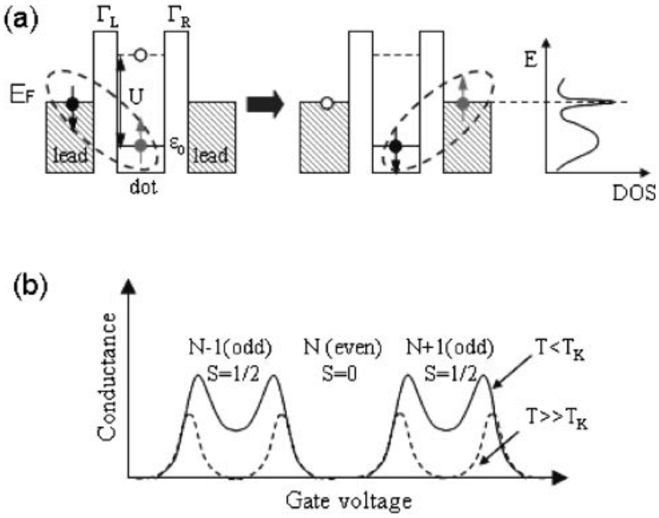

Fig. 1. (a) Schematic energy diagram of a quantum dot coupled with the source and drain leads via tunnel barriers. The dot has spin $S = 1/2$ when an uppermost level has an unpaired electron. The Kondo effect enhances the conductance through higher order tunneling of anti-ferromagnetically correlated spin pairs at $T < T_K$. (b) Coulomb blockade oscillations for $T \gg T_K$ (dashed line) and for $T < T_K$ (solid line). The conductance of only the odd N valleys increase due to the Kondo effect.

(DOS) at the Fermi energy. Therefore, the conductance starts to increase at $T \sim T_K$. This behaviour is qualitatively opposite to that in bulk metal because the current path is only through the "magnetic impurity" in the case of the quantum dot. The Kondo temperature, T_K, is given as

$$T_K = \frac{\sqrt{\Gamma U}}{2} \exp[-\pi(E_F - \varepsilon_0)(U - E_F + \varepsilon_0)/\Gamma U], \quad (1)$$

where $\Gamma = \Gamma_L + \Gamma_R$. The above second order tunneling occurs coherently and tends to screen the initial localized magnetic moment in the dot through the dot-lead spin singlet formation. Figure 1(b) shows the Kondo effect theoretically

*E-mail: satoshi@nttbrl.jp

predicted for Coulomb oscillations in a quantum dot.[4)] Regular Coulomb oscillations, which appear at temperature $> T_K$, are significantly modified as the temperature becomes comparable to or lower than T_K. In the region of the conductance valley (Coulomb valley), the number of electrons, N, in the dot is fixed to an integer. However, the valley conductance for odd N with $S = 1/2$ increases and finally reaches the unitary limit (linear conductance $= 2e^2/h$ when $\Gamma_L = \Gamma_R$).[4,5)]This is not the case for the valley holding even N with $S = 0$. In most of quantum dots, however, T_K is too low to visualize the Kondo effect in the experimentally available temperature range ($T > 10\,\mathrm{mK}$). So the Kondo effect is only observed in a quantum dot having a smaller size and stronger couplings to the leads, i.e., larger U and Γ values.[2)] Another way to raise the Kondo temperature is to increase the number of states involved in such virtual tunneling processes that build up the Kondo many-body state.[6–8)] In quantum dots, the electronic states can be varied as a function of N and magnetic field, B. This allows us to tune the degeneracy of many-body states contributing to the Kondo effect. We previously observed a strong enhancement of the Kondo effect for degeneracy of two-electron states between a spin singlet and triplet states.[9)] In this work, we use a vertical quantum dot to study the Kondo effect. The number of electrons, N, in this dot is precisely varied as a function of plunger gate voltage, starting from zero. In addition, the lateral confining potential is well approximated by a two-dimensional (2D) harmonic function so that the electronic configuration can be well analyzed.[10)] We control over the spin configuration in the few electron regime as a function of gate voltage and magnetic field.[11)] We find strong enhancement of the Kondo effect induced by degeneracy between a spin singlet and a triplet states ("S–T Kondo effect") and between two spin doublet states ("D–D Kondo effect").[12)] We compare the features of the Kondo effect between these two cases.

2. Tunable State Degeneracy and Spin Configuration

Electronic states in quantum dots are determined to minimize the total energy or sum of the quantum mechanical energy and interaction energy. The spin state, thus determined, usually takes a total spin, $S = 0$ when N is even, and $S = 1/2$ when N is odd. S can be greater than $1/2$ when the spin-related interaction is strong. We have previously studied the filling of a vertical quantum dot, and found that the electronic configuration is significantly modified for the filling of nearly degenerate orbital states. The orbital degeneracy can be adjusted as a function of magnetic field B. This allows us to investigate the Kondo effect for tunable electronic configurations.

Here we assume two orbital states crossing with each other at a magnetic field of $B = B_0$. By taking into account spin degeneracy, these orbital states are consecutively filled by four electrons in total. If these are the electrons from the $(N+1)$th to the $(N+4)$th for filling the dot, the corresponding electrochemical potentials are defined as $\mu(N+1)$, $\mu(N+2)$, $\mu(N+3)$ and $\mu(N+4)$, respectively, and they are schematically shown in Fig. 2(a). The electrochemical potential $\mu(N)$ is defined as $\mu(N) = U(N) - U(N-1)$, where $U(N)$ is the total energy for a quantum dot holding N electrons. $\mu(N+1)$ just traces the orbital state with the lower energy. If we assume N is even, this ground state (GS) is a spin doublet having $S = 1/2$. The $N+2$ electron GS with $\mu(N+2)$ is a spin singlet state ($S = 0$) having two anti-parallel spins in a single orbital state for B far away from B_0. However, close to the point of $B = B_0$, the GS is a spin triplet state ($S = 1$) having parallel spins in two different orbital states, following Hund's rule.[10,11)] The triplet GS is signified by a downward cusp both ended by an upward cusp, indicating a singlet–triplet transition. Here, we neglect the Zeeman energy. The $N+3$ electron GS with $\mu(N+3)$ is a spin half state ($S = 1/2$) having a filled spin-degenerate orbital state, and the $N+4$ electron GS with $\mu(N+4)$ is formed by filling all of the available states. Note the two dash-dotted lines in Fig. 2(a) show degeneracy of two doublet states for the $N+1$ and $N+3$ GSs, and the two dotted lines show degeneracy of a singlet and triplet states for the $N+2$ GS. We focus on all of these degenerate points in the experiment on the Kondo effect as described later.

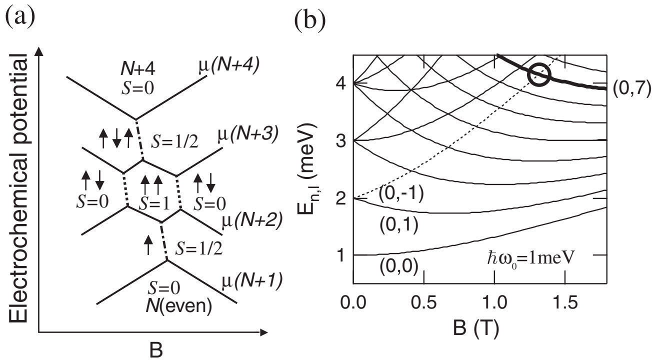

Fig. 2. (a) Schematic magnetic field dependence of the electrochemical potential for electron numbers from $N+1$ (odd) to $N+4$ (even) occupying two crossing orbitals. A triplet state ($S = 1$) appears around the level crossing field at $N+2$. (b) Fock–Darwin states calculated with $\hbar\omega_0 = 1\,\mathrm{meV}$. The circle denotes crossing between orbital state $(n,l) = (0,-1)$ (dotted line) and $(0,7)$ (thick solid line) where the Kondo effect for $N = 15$ and 16 are studied in detail.

Our model of electrochemical potentials is so simple, however, it reproduces well an experiment on a circular 2D quantum dot.[11)] Figure 3 shows the experimental data of Coulomb peaks evolving with magnetic field between $N = 0$ and 14. The device used for this experiment is a $0.5\,\mu\mathrm{m}$ diameter circular mesa of a $7.5\,\mathrm{nm}$ $Al_{0.22}Ga_{0.78}As$/$12\,\mathrm{nm}$ $In_{0.05}Ga_{0.95}As$/$9.0\,\mathrm{nm}$ $Al_{0.22}Ga_{0.78}As$ double barrier structure (DBS). A source and drain contacts are located below and above the DBS, respectively, and a gate electrode is placed on the side of the mesa (see inset to Fig. 4). A 2D harmonic dot is located between the two AlGaAs barriers. The device is mounted in a dilution refrigerator with a base temperature of $50\,\mathrm{mK}$, and a vertically flowing current in response to a dc excitation voltage, V_{sd}, of $120\,\mu\mathrm{V}$ is measured as a function of gate voltage. Then a series of current peaks, i.e., Coulomb peaks, appear corresponding to a one-by-one change in the electron number N in the dot. Note this quantum dot is so weakly coupled to the contact leads that the Kondo effect is not observed as described before. The position of a Coulomb peak for the transition from $N-1$ to N measures the electrochemical potential $\mu(N)$. We see large peak spacings for $N = 2$ and 6 at $B = 0$ due to the shell filling and also for $N = 4$ due to Hund's rule,

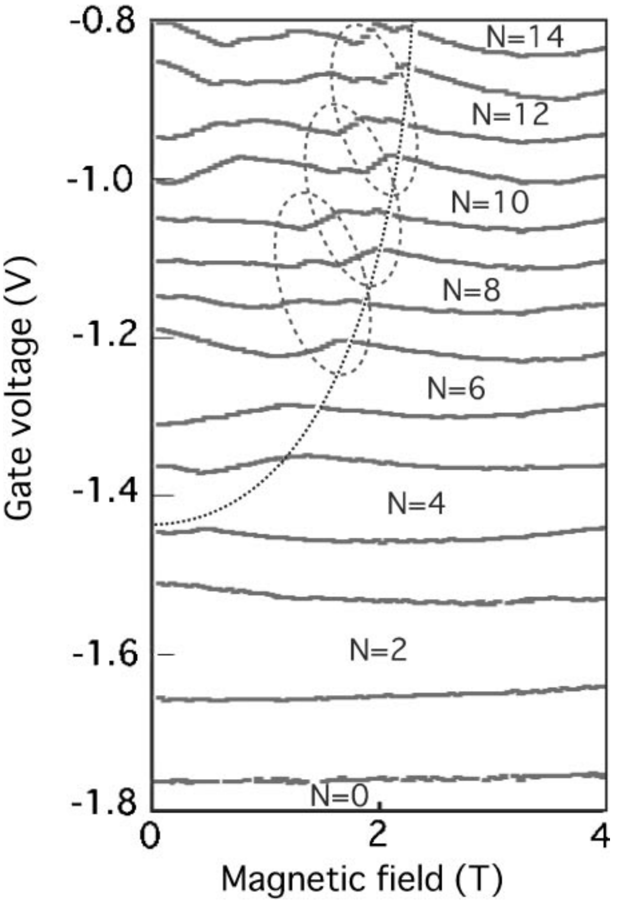

Fig. 3. Evolution of current peaks for $N = 1$ to 14 with magnetic field measured for $V_{sd} = 120\,\mu V$. The dotted line indicates the magnetic field of the filling factor $\nu = 2$. Dotted ovals indicate the regions where two crossing Fock–Darwin states are consecutively filled by four electrons. The four peak lines to the top in each oval correspond to electrochemical potentials of $\mu(N+1)$ to $\mu(N+4)$, respectively.

and evolution of neighboring peaks in pairs with magnetic field due to consecutive anti-parallel spin filling of a single orbital state.

The eigenstates confined by a 2D harmonic potential in the presence of a magnetic field perpendicular to the 2D plane of the dot are the Fock–Darwin (FD) states with energies $E_{n,l}$.[13] $E_{n,l}$ is shown in Fig. 2(b);

$$E_{n,l} = -\frac{l}{2}\hbar\omega_c + \left(n + \frac{1}{2} + \frac{1}{2}|l|\right)\hbar\sqrt{4\omega_0^2 + \omega_c^2}, \qquad (2)$$

where $n = 0, 1, 2, \dots$ is the radial quantum number and $l = 0, \pm1, \pm2, \dots$ is the angular quantum number. $\hbar\omega_0$ is the lateral confinement energy and $\hbar\omega_c = eB/m^*$. Zeeman splitting is neglected, so each state is two-fold degenerate. The evolutions of the paired lines in Fig. 3 are well reproduced by the FD diagram. Note crossing of the FD states, or orbital and spin degeneracy, is lifted by the interaction effect in Fig. 3. So the wiggles or anti-crossings between pairs of peaks correspond to the crossings of FD states. Modifications to the simple pairing of peaks are observed in each dashed oval connecting pairs of peaks along the dashed line at non-zero field. This oval indicates the four-electron filling at the crossing of two FD states, and the four peak lines inside the oval are well reproduced by our electrochemical potential model of Fig. 2(a).

3. The Kondo Effect Enhanced by State Degeneracy

We use a technique of manipulating S–T and D–D degeneracies described in the preceding section to study the Kondo effect in our quantum dot device. Here we also use a vertical quantum dot but having a much stronger coupling between the dot and contact leads. The tunnel barriers are made from two 7-nm-thick $Al_{0.06}Ga_{0.94}As$. The built-in dot-lead coupling Γ via the AlGaAs barriers for this dot device is $400\,\mu eV$ for the first electron entering the dot, and gradually increases as N increases. As described before, the values of S and N can be unambiguously determined in this quantum dot. All the transport measurements were performed in a dilution refrigerator with a base temperature of $\simeq 60\,mK$, using a standard lock-in technique with an ac excitation voltage between source and drain of $3\,\mu V$. This excitation voltage is much smaller than $k_B T_K$.

Figure 4 shows a gray-scale plot of the linear conductance, G, as a function of V_g and B at the base temperature. White stripes indicate Coulomb peaks between $N = 0$ and 21. The overall features observed here such as shell filling and spin pairing are consistent with those in Fig. 3. The magnetic evolutions of the peak pairs are assigned to successive filling of FD states[13] by spin-up and -down electrons.

On the other hand, marked difference from Fig. 3 is observed for $V_g > -1.0\,V$. We see many white vertical lines connecting neighboring Coulomb peaks in the regions where pairs of peaks become close to each other. These vertical lines indicate lifting of Coulomb blockade due to the Kondo effect. There are more such lines as V_g increases, because in

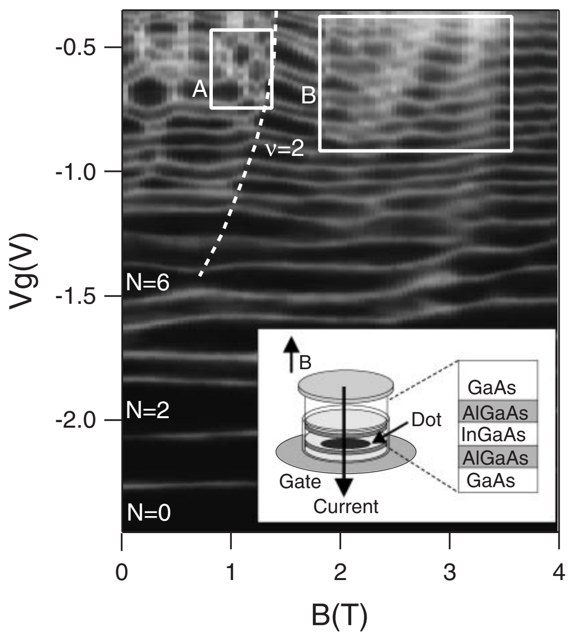

Fig. 4. Gray-scale plot of the linear conductance as a function of the magnetic field and gate voltage, or B–N diagram. Black corresponds to zero conductance, and white to $G = 50\,\mu S$. All the electrons occupy the first Landau level on the right hand side of the dashed line (filling factor $\nu = 2$). The magnetic field induced Kondo effect is observed within region A. Spin flip transitions occur within region B until completely spin polarized $\nu = 1$ state is reached. The inset shows a schematic diagram of the dot structure made from AlGaAs/InGaAs/AlGaAs double barrier tunnel-diode.

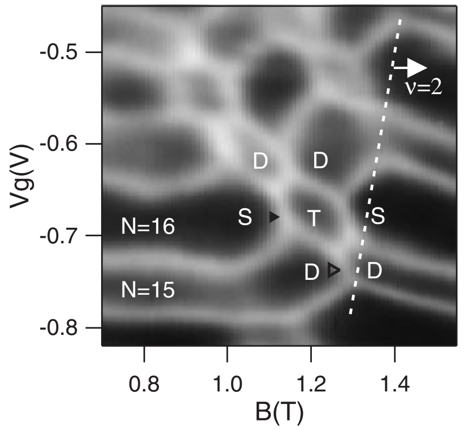

Fig. 5. Detailed measurement conducted in region A in Fig. 4. The gray-scale is same as in Fig. 4. S, T and D denote states with $S = 0$ (singlet), $S = 1$ (triplet) and $S = 1/2$ (doublet). The enhanced conductance due to the Kondo effect is observed in the Coulomb valley corresponding to the dotted and dash-dotted lines in Fig. 2(a).

our quantum dot device, Γ gradually increases with increasing V_g.

Figure 5 shows detailed measurement conducted in region A marked in Fig. 4. The last orbital crossings occur between $E_{n,l}$ states with $(n, l) = (0, -1)$ and $(0, l)$ $(l > 1)$ on the dotted line, and all the electrons occupy the ground Landau level at higher B $(\nu = 2)$. A spin triplet state is observed at $N = 16$ and $B \simeq 1.2\,\mathrm{T}$, where states $(n, l) = (0, -1)$ and $(0, 7)$ are occupied by electrons having parallel spins [see the circle in Fig. 2(b)]. When we compare the white lines in Fig. 5 with the electrochemical potentials vs B in Fig. 2(a), we find that the white vertical lines in Fig. 5 fall onto the dotted and dash-dotted lines in Fig. 2(a). For example, in the $N = 16$ Coulomb valley, the conductance is enhanced at $B \simeq 1.1\,\mathrm{T}$ and $B \simeq 1.3\,\mathrm{T}$ corresponding to the dotted lines in Fig. 2(a) where the singlet and triplet GS are degenerate. These are both assigned to the S–T Kondo effect. The Kondo temperature, $T_K^{S\text{–}T}$, is considerably higher than the conventional $S = 1/2$ Kondo temperature, T_K^D, because of the larger degeneracy.[9] As for $N = 15$ and 17, the conventional $S = 1/2$ Kondo effect is expected. However, the conductance enhancement in the Coulomb valleys is not clearly observed except in the regions corresponding to the dash-dotted lines in Fig. 2(a), where two $S = 1/2$ states with different total angular momentum, M, are degenerate. When such an orbital degeneracy is present for odd N, a total of four states, i.e., $M = M_1$, M_2 $(M_1 \neq M_2)$, $S_Z = \pm 1/2$, are involved in forming the Kondo singlet state if the Zeeman splitting is negligible. Then, an enhancement of T_K is expected reflecting this four-fold degeneracy as in the S–T Kondo effect. We refer this type of Kondo effect for odd N to "doublet–doublet" (D–D) Kondo effect.[12] Because T_K^D is much lower than the D–D Kondo temperature, $T_K^{D\text{–}D}$, only a slight conductance enhancement is observed in the odd N Coulomb valleys when there is no orbital degeneracy. Since many orbital crossings occur before the system enters the $\nu = 2$ regime, a honeycomb pattern is formed in a B–N diagram by the high conductance region, provided $T_K^D < T < T_K^{S\text{–}T}, T_K^{D\text{–}D}$. Such honeycomb pattern is clearly captured in Fig. 5, due to the S–T and D–D Kondo effects that occur consecutively for different orbital crossings.

Our honeycomb pattern is different from "chessboard pattern" discussed in a lateral quantum dot.[14–17] In a vertical quantum dot, one can assume that the orbital quantum numbers are conserved in tunnel processes between the dot and leads due to their same rotational symmetry. Hence we expect "two channels" of conduction electrons in the leads when two orbitals are relevant in the quantum dot; each channel couples to only one of the two orbitals. On the other hand, a "single channel" in the leads preferentially couples to the outer orbital in the case of a lateral quantum dot. Then, high-conductance Coulomb valleys appear alternately in B–N diagram due to the Kondo effect involving electrons in the outer orbital.

Figures 6(a) and 6(b) show temperature dependence of the differential conductance dI/dV_{sd} vs V_{sd} for the S–T $(N = 16)$ and D–D $(N = 15)$ Kondo effect, respectively. The gate voltage is fixed in the center of the respective Coulomb valley (solid and open triangle in Fig. 5). A clear Kondo peak at $V_{sd} = 0\,\mathrm{V}$ is observed at low temperatures, whose height decreases with increasing temperature as expected for the Kondo effect.

After a background subtraction of non-Kondo cotunneling component,[18] the above temperature dependence of the Kondo peak height is fitted to the function

$$\frac{G}{G_0} = \left\{ \frac{T_K'^2}{T^2 + T_K'^2} \right\}^s, \tag{3}$$

where G_0 is the low temperature limit conductance and $T_K' = T_K/\sqrt{2^{1/s} - 1}$.[19,20] G_0 does not reach the unitary limit conductance of $2e^2/h$[5] probably because of the asymmetry in the two tunnel barriers; it is impossible to tune Γ to the upper and lower leads separately in our vertical quantum dot because Γ is pre-determined by the growth parameter of the

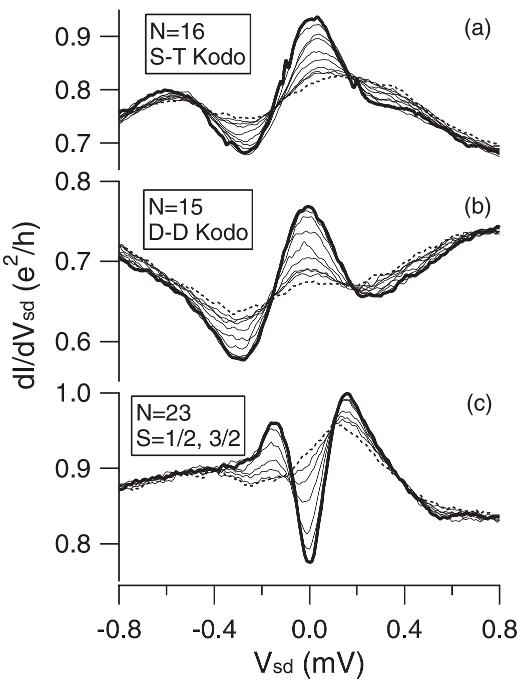

Fig. 6. Temperature dependence of the differential conductance dI/dV_{sd} vs V_{sd} from $T = 60\,\mathrm{mK}$ (thick solid line) to 1.5 K (dotted line) for (a) S–T Kondo effect, (b) D–D Kondo effect and (c) $S = 1/2$–$S = 3/2$ degeneracy.

material. The T_K^{S-T} and T_K^{D-D} estimated from the curve fitting are 700 mK and 490 mK, respectively. The higher T_K for the S–T Kondo effect may be due to the larger Γ, and it is difficult to experimentally determine which is larger, T_K^{S-T} or T_K^{D-D}, for the same Γ. The fitted values of the parameter s are 0.8 for the S–T Kondo effect and 1.1 for the D–D Kondo effect, much larger than $s \simeq 0.2$ for a conventional spin 1/2 system. However, the estimation of s is less reliable because it changes substantially with the chosen fitting range. The expected Zeeman splitting of $\simeq 30\,\mu$eV at $B \simeq 1.2$ T is smaller than T_K estimated above. Therefore, a Zeeman splitting in the dI/dV_{sd} Kondo peak is not resolved, and we are allowed to treat all four S–T and D–D states as quasi-degenerate.

Figures 7(a) and 7(b) show a gray-scale plot of dI/dV_{sd} in B–V_{sd} plane for the S–T Kondo effect ($N = 16$) and for the D–D Kondo effect ($N = 15$), respectively, with V_g fixed in the center of the respective Coulomb valley. Conductance peaks at $V_{sd} = 0$ V are observed near the degeneracy field, B_0 ($B_0 = 1.255$ T for D–D, 1.12 and 1.25 T for S–T). The two zero-bias S–T Kondo peaks in Fig. 7(a) correspond to the two conductance maxima in the $N = 16$ Coulomb valley (see Fig. 5). Because the S–T or D–D degeneracy is lifted as $|\Delta B| = |B - B_0|$ increases, the Kondo effect is broken and the zero-bias peak is suppressed. At large $|\Delta B|$, a peak or step is observed at $eV_{sd} = \pm\Delta$ where the brightness suddenly changes. Here, Δ is the B-dependent energy difference between the singlet and triplet states, or between the two doublet states. This peak/step is due to cotunneling associated with the two states separated by Δ,[9] and therefore observed within the Coulomb valley ($\simeq 0.6$ meV).

Figure 8(a) shows V_{sd} values of the conductance peak/step as a function of ΔB. Peak/step positions for both the S–T ($B_0 = 1.12$ T) and the D–D ($B_0 = 1.25$ T) Kondo effect almost coincide, indicating that they involve the same orbital states, namely $(n, l) = (0, -1)$ and $(0, 7)$.

Figure 8(b) compares the relative conductance, ΔG, measured from the degeneracy ($\Delta B = 0$) at $V_{sd} = 0$ V, as a function of ΔB. The scaling calculation[8,21] has shown that, in the S–T Kondo effect, $T_K(\Delta)$ obeys a power law $T_K(\Delta) = T_K(0) \cdot (T_K(0)/\Delta)^\gamma$ with $\gamma = 2 + \sqrt{5}$ on the triplet side, whereas $T_K(\Delta)$ drops to zero suddenly on the singlet side. The observed S–T Kondo peak conductance drops more quickly on the singlet side ($\Delta B < 0$) than on the triplet side ($\Delta B > 0$) reflecting the asymmetric behavior of T_K given by the scaling calculation.

Another scaling calculation was recently applied to the D–D Kondo effect,[12,22] and $\gamma = 1$ was obtained in the case of an equivalent dot-lead coupling for the two orbitals involved. The observed D–D Kondo peak conductance

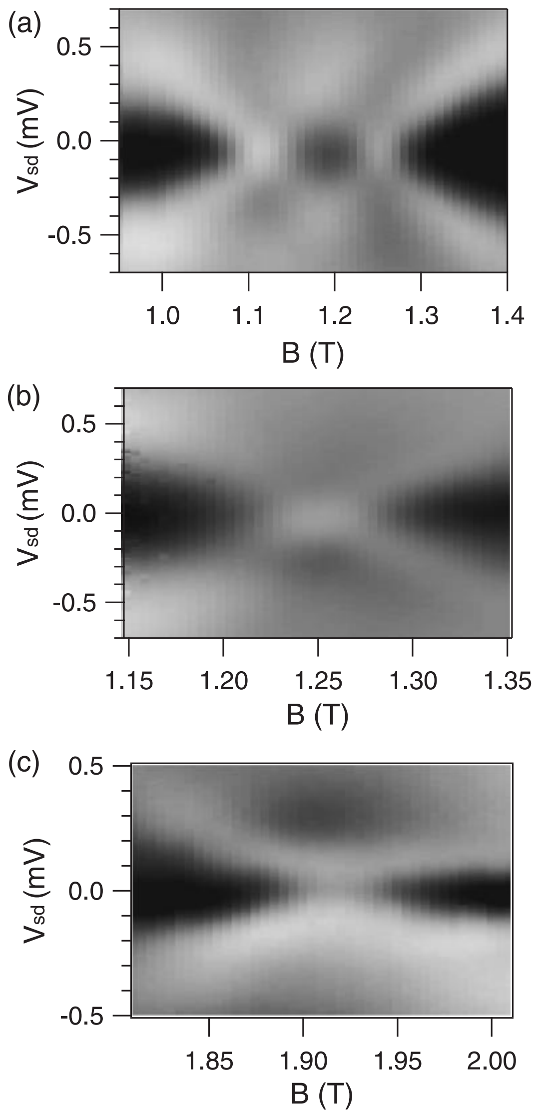

Fig. 7. Gray-scale plot of dI/dV_{sd} in B–V_{sd} plane for (a) the S–T Kondo effect at $N = 16$, (b) the D–D Kondo effect at $N = 15$ and (c) $S = 1/2$–$S = 3/2$ degeneracy at $N = 21$. V_g is fixed in the center of the respective Coulomb valley. Black corresponds to $G = 10\,\mu$S in (a) and (b), and to $G = 25\,\mu$S in (c). White corresponds to $G = 45\,\mu$S in all three cases.

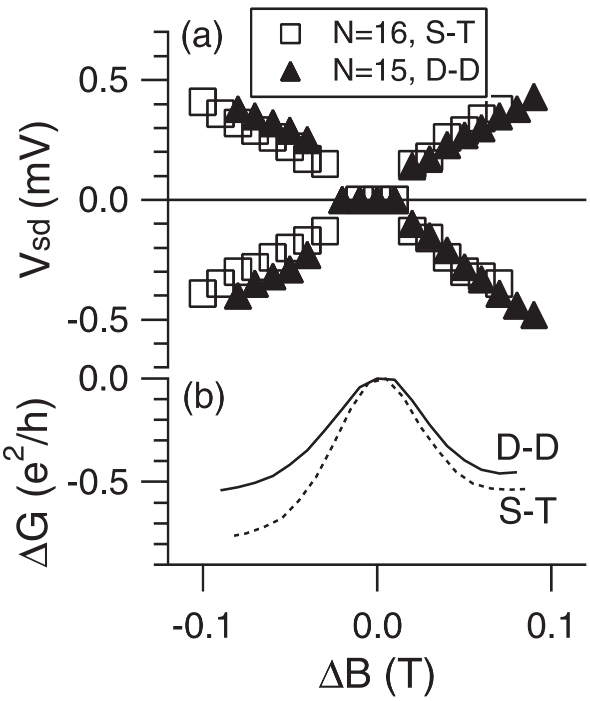

Fig. 8. (a) V_{sd} values of the conductance peak or step obtained from Fig. 7 as a function of the magnetic field difference $\Delta B = B - B_0$, where B_0 is the degeneracy magnetic field. (b) Relative conductance measured from the degeneracy ($\Delta B = 0$) at $V_{sd} = 0$ V, for the D–D (solid line) and the S–T (dotted line) Kondo effect.

drops more slowly and symmetrically compared to the S–T Kondo case, i.e., $T_K^{D–D}$ is more robust against degeneracy lifting than $T_K^{S–T}$, in qualitative agreement with the theory. Please note that, in Fig. 5, the width of the enhanced conductance region, or a "bridge" between the Coulomb peaks, is consistently larger for the D–D Kondo effect [the dot-dashed line in Fig. 2(a)] than for the S–T Kondo effect [the dotted line in Fig. 2(a)] at other N as well.

When all the electrons occupy the ground Landau level ($\nu = 2$), the spin state is doublet (singlet) for odd (even) N. The system then enters a spin flip region ("B" in Fig. 4) when B further increases, and finally reaches a totally spin polarized state ($\nu = 1$), or maximum density droplet (MDD).[23] The first spin-flip transition occurs at $B \simeq 2.0\,\mathrm{T}$ from $S = 0$ to 1 for even N, and from $S = 1/2$ to $3/2$ (quadruplet) for odd N within region B. This spin transition in the GS is clearly signaled by the kink in the Coulomb peak evolution with B as well as by the Kondo effect; the S–T Kondo effect is observed for even N as the enhanced conductance in the Coulomb valley suggests. A similar conductance enhancement is observed in the Coulomb valley for the doublet–quadruplet (D–Q) degeneracy with odd N, suggesting a D–Q Kondo effect. However, a zero-bias peak is not observed in the differential conductance characteristic shown in Fig. 6(c). On the contrary, a zero-bias "dip" develops at low temperatures. In this particular case of D–Q degeneracy at $N = 23$, the transition occurs from a doublet state where $(n, l) = (0, 11)$ state is occupied by an unpaired electron, to a quadruplet state where $(n, l) = (0, 10)$, $(0, 11)$ and $(0, 12)$ states are each occupied by an unpaired electron. Figure 7(c) shows the B-dependence of the differential conductance characteristic, where the D–Q degeneracy occurs at $B = 1.91\,\mathrm{T}$ and $N = 21$. Temperature dependence of the differential conductance characteristic similar to Fig. 6(c) is observed for this electron number as well, although the overall feature is more asymmetric. Unlike the two-stage Kondo effect reported in a lateral quantum dot,[24] no peak is found at $V_{sd} = 0\,\mathrm{V}$ even when B is scanned across the transition point, and the D–Q degeneracy remains as a saddle point in the B–V_{sd} diagram. The peaks in the differential conductance in Fig. 6(c) roughly corresponds to three times the Zeeman splitting at this magnetic field. Although the peaks may be related to the Zeeman splitting between $S_Z = 3/2$ and $-3/2$ states, we have no clear explanation as yet for the above observed features.

4. Conclusion

In conclusion, we have observed a strong Kondo effect in a two-dimensional harmonic quantum dot when a magnetic field induces state degeneracies between a spin singlet and triplet states and between two spin doublet states. The estimated Kondo temperature is comparable between the two kinds of degeneracies but much higher than that for a standard spin-half Kondo effect, indicating that a total of four-fold spin and orbital degeneracy for both cases accounts for the similar enhancement of the Kondo temperature. In addition, for degeneracy between a spin doublet and quadruplet states, we have observed enhanced conductance in the Coulomb valley but a zero bias dip. This can be due to the Zeeman splitting, but the physics is not yet clear.

Acknowledgment

The authors acknowledge valuable discussions with M. Eto, S. Amaha, W. Izumida, L. I. Glazman, H. Hyuga, M. Stopa and J. Kondo. The work is supported by the financial support from the Grant-in-Aid for Scientific Research A (No. 40302799) and from CREST-JST.

1) J. Kondo: Prog. Theor. Phys. **32** (1964) 37.
2) D. Goldhaber-Gordon, H. Shtrikman, D. Mahalu, D. Abusch-Magder, U. Meirav and M. A. Kastner: Nature **391** (1998) 156; S. M. Cronenwett, T. H. Oosterkamp and L. P. Kouwenhoven: Science **281** (1998) 540; J. Schmid, J. Weiss, K. Ebel and K. von Klitzing: Physica B **256–258** (1998) 182.
3) L. I. Glazman and M. E. Raikh: JETP Lett. **47** (1988) 452; T. K. Ng and P. A. Lee: Phys. Rev. Lett. **61** (1988) 1768.
4) A. Kawabata: J. Phys. Soc. Jpn. **60** (1991) 3222; W. Izumida, O. Sakai and Y. Shimizu: J. Phys. Soc. Jpn. **67** (1998) 2444.
5) W. G. van der Wiel, S. De Franceschi, T. Fujisawa, J. M. Elzerman, S. Tarucha and L. P. Kouwenhoven: Science **289** (2000) 2105.
6) T. Inoshita, A. Shimizu, Y. Kuramoto and H. Sakaki: Phys. Rev. B **48** (1993) 14725.
7) M. Eto and Y. V. Nazarov: Phys. Rev. Lett. **85** (2000) 1306; M. Eto and Y. V. Nazarov: Phys. Rev. B **64** (2001) 085322.
8) M. Eto and Yu. V. Nazarov: Phys. Rev. B **66** (2002) 153319.
9) S. Sasaki, S. De Franceschi, J. M. Elzerman, W. G. van der Wiel, M. Eto, S. Tarucha and L. P. Kouwenhoven: Nature **405** (2000) 764.
10) S. Tarucha, D. G. Austing, T. Honda, R. J. van der Hage and L. P. Kouwenhoven: Phys. Rev. Lett. **77** (1996) 3613.
11) S. Tarucha, D. G. Austing, Y. Tokura, W. G. van der Wiel and L. P. Kouwenhoven: Phys. Rev. Lett. **84** (2000) 2485.
12) S. Sasaki, S. Amaha, N. Asakawa, M. Eto and S. Tarucha: Phys. Rev. Lett. **93** (2004) 17205.
13) V. Fock: Z. Phys. **47** (1928) 446; C. G. Darwin: Proc. Cambridge Philos. Soc. **27** (1930) 86.
14) M. Keller, U. Wilhelm, J. Schmid, J. Weis, K. v. Klitzing and K. Ebel: Phys. Rev. B **64** (2001) 033302.
15) C. Fühner, U. F. Keyser, R. J. Haug, D. Reuter and A. D. Wieck: Phys. Rev. B **66** (2002) 161305(R).
16) U. F. Keyser, C. Fuhner, S. Borck, R. J. Haug, M. Bichler, G. Abstreiter and W. Wegscheider: Phys. Rev. Lett. **90** (2003) 196601.
17) M. Stopa, W. G. van der Wiel, S. De Franceschi, S. Tarucha and L. P. Kouwenhoven: Phys. Rev. Lett. **91** (2003) 046601.
18) L. I. Glazman and M. Pustilnik: in *New Directions in Mesoscopic Physics (Towards Nanoscience)*, ed. R. Fazio, V. F. Gantmakher and Y. Imry (Springer, Heidelberg, 2004) NATO Science Serees II, Vol. 125.
19) D. Goldhaber-Gordon, J. Gores, M. A. Kastner, H. Shtrikman, D. Mahalu and U. Meirav: Phys. Rev. Lett. **81** (1998) 5225.
20) T. A. Costi and A. C. Hewson: Philos. Mag. B **65** (1992) 1165.
21) M. Pustilnik and L. I. Glazman: Phys. Rev. Lett. **85** (2000) 2993; M. Pustilnik and L. I. Glazman: Phys. Rev. B **64** (2001) 045328.
22) M. Eto: J. Phys. Soc. Jpn. **74** (2004) 95.
23) T. H. Oosterkamp, J. W. Janssen, L. P. Kouwenhoven, D. G. Austing, T. Honda and S. Tarucha: Phys. Rev. Lett. **82** (1999) 2931.
24) W. G. van der Wiel, S. De Franceschi, J. M. Elzerman, S. Tarucha, L. P. Kouwenhoven, J. Motohisa, F. Nakajima and T. Fukui: Phys. Rev. Lett. **88** (2002) 126803.

Satoshi Sasaki was born in Tokyo, Japan in 1965. He received his B. Sc. (1988), M.E. (1990) and Ph. D. (1993) degrees from University of Tokyo. He joined NTT Basic Research Laboratories in 1993. Since then, he has studied transport properties of mesoscopic devices, especially quantum dots. He is a member of the Physical Society of Japan and the Japan Society of Applied Physics.

Seigo Tarucha received the B.E. and M.S. degrees in applied physics from the University of Tokyo in 1976 and 1978, respectively. He joined NTT Basic Research Laboratories in 1978 and received his Ph. D. degree in applied physics from the University of Tokyo in 1986. In 1998 he moved to the University of Tokyo as a professor in the Department of Physics, and in 2004 to the Department of Applied Physics. He was a guest scientist in Max-Planck-Institut fuer Festkoerperforschung, Stuttgart, Germany during 1986–1987, and a visiting professor in the Delft University of Technology, the Netherlands in 1995. Since 1986 he has carried out experimental research on ballistic and quantum transport in semiconductor nanostructures such as quantum wells, wires and dots. His current interest is in spin correlation effects and quantum coherence in semiconductor quantum dot structures, and physics and technologies of spin-based quantum computing. He is an editor of Semiconductor Science and Technology, and a member of the Physical Society of Japan and the Japan Society of Applied Physics.